Optics Letters

Rotation-dependent nonlinear absorption of orbital angular momentum beams in ruby

G. Musarra,[1] K. E. Wilson,[2] D. Faccio,[1,*] and E. M. Wright[2,3]

[1]School of Physics and Astronomy, University of Glasgow, Glasgow G12 8QQ, UK
[2]School of Engineering and Physical Sciences, Heriot-Watt University, Edinburgh EH14 4AS, UK
[3]College of Optical Sciences, University of Arizona, Tucson, Arizona 85721, USA
*Corresponding author: daniele.faccio@glasgow.ac.uk

Received 16 April 2018; revised 26 May 2018; accepted 26 May 2018; posted 29 May 2018 (Doc. ID 328409); published 21 June 2018

We investigate the effect of a rotating medium on orbital angular momentum (OAM)-carrying beams by combining a weak probe beam shifted in frequency relative to a strong pump beam. We show how the rotational Doppler effect modifies the light-matter interaction through the external rotation of the medium. This interaction leads to an absorption that increases with the mechanical rotation velocity of the medium and with a rate that depends on the OAM of the light beam.

OCIS codes: (190.5940) Self-action effects; (080.4865) Optical vortices; (260.1180) Crystal optics; (190.4223) Nonlinear wave mixing.

https://doi.org/10.1364/OL.43.003073

The rotational Doppler effect is the rotational counterpart of the translational Doppler effect that arises when the source is in relative rotation with respect to the observer. Originally introduced by Garetz [1], this phenomenon is typically observed with angular momentum-carrying beams propagating in a rotating medium [2,3]: in this case, the rotation induces a frequency shift in the observed beam that is proportional to both the rotational rate and the angular momentum state [4], thus allowing, for example, for the measurement of the rotational speed of a remote rotating object [5]. The effects of the rotational Doppler shift have also been observed due to the rotational motion of atomic particles [6,7] in rotational Raman scattering [1] and in nonlinear optics with applications in second-harmonic generation [8] and predictions of parametric amplification of light from mechanical rotation [9]. Since the rotational Doppler effect is associated with the angular momentum of the beam [4,10–12], it will arise with a spin or with orbital angular momentum (OAM) states.

The rotational Doppler effect with OAM-carrying beams has been observed optically [13,14] and proposed for remote detection of rotation in both terrestrial and astronomical objects [5]. Its effect has been enhanced in specific materials such as ruby where the observed light-dragging effect allows demonstration of phenomena such as the mechanical Faraday effect for OAM beams [15] and for structured beams [16]. These effects were interpreted as the result of slow light propagation in ruby which, in turn, has been described as originating from a coherent population oscillation in the medium and a corresponding narrow-band change in the refractive index that can explain the large group refractive indices [17–19]. It is worth noting, however, that other models have also been proposed that rely only on the *incoherent* saturable absorption properties of ruby and lead to similar results without requiring coherent population oscillations within the medium [20]. Both models provide the same intensity dependence for the light-dragging effect.

Regardless of the controversy around the details that lead to light-dragging or slow light effects in ruby [20], all proposed models lead to the same conclusion when we consider only the changes in absorption due to a periodic modulation of an intense beam propagating through a saturable-absorbing medium. For example, the incoherent bleaching model [21–23] couples the ground state population with the pump beam intensity evolution and predicts that a weak periodic modulation of the pump beam will modify the saturated absorption coefficient, leading to an increasing absorption for increasing modulation frequency. In most experiments, modulation of the pump beam is obtained by direct amplitude modulation of the beam with, e.g., an acousto-optic modulator [17,20].

In this Letter, we investigate the effect on an OAM-carrying probe beam of a rotating ruby rod using a Gaussian-shaped pump beam. Amplitude modulation of the pump beam is obtained by introducing a probe beam that carries OAM. Therefore, the probe beam frequency is rotationally Doppler shifted by the ruby rod rotation, creating the conditions for absorption modulation, as discussed above. Our results, therefore, show increasing absorption for the increasing mechanical rotation speed of the medium, with a rate that increases with increasing OAM of the light beam. This furnishes an additional example of how the rotational Doppler effect combines with light-matter interactions due to external rotation.

An intuitive picture of the rotational equivalent to the Doppler effect is given by considering that the light transmitted in a rotating medium is dragged by that medium [24], giving rise to an angular frequency shift, as happens also to the hands of a clock on a rotating table. In the following, we deal with helically symmetric beams for which the winding number ℓ is proportional to the OAM. When the beam has both spin and OAM, the frequency shift $\Delta\omega$ is given by

$$\Delta\omega = (\sigma + \ell) \cdot \Omega, \quad (1)$$

where σ and ℓ, respectively, are the spin and the OAM of the beam, and Ω is the rotating frequency of the medium [5]. In our experiments, for the pump and the probe, we chose the same circular polarization, but different OAM, so the total frequency shift between the pump and the probe is

$$\Delta\omega = \Delta\ell \cdot \Omega, \quad (2)$$

where $\Delta\ell$ is the difference between the probe and the pump OAM value. By using the beam with OAM $\ell = 0$ as an intense pump, we then investigated the effect of a rotating ruby rod on the OAM-carrying probe beam by measuring the transmitted intensity T of the probe as a function of the rotational speed Ω of the medium. In this case, we examine four different values of OAM from $\ell = 1$ to $\ell = 4$.

The full experimental layout is shown in Fig. 1. A linearly polarized, continuous-wave laser with carrier wavelength ($\lambda = 532$ nm) propagates through the half-wave plate (HWP) and the polarizing beam splitter (PBS) to control the overall input beam power. Then the light beam propagates through the diffraction grating DG with a fork dislocation centered on the beam axis that converts the Gaussian beam into OAM modes. The diffracted beams pass through a PBS, and a quarter-wave plate (QWP) transforms to circular polarization so as to ensure a rotation-invariant interaction with the birefringent ruby crystal when this rotates. The convex lens L1 of focal length $f = 1000$ m focuses the beams, and the two pinholes $PH_{\ell=0}$ and $PH_{\ell=1,2,3,4}$ spatially select the pump and the probe beams, respectively. The probe power was set to 70 mW for all ℓ values. Since the OAM probe beams have different sizes for different ℓ, the pump power was controlled with a variable transmission filter so as to guarantee equal nonlinear interaction for each ℓ. In order to obtain constant pump intensities in the four OAM states, the pump power was set to 390, 420, 561, and 624 mW for $\ell = 1$, 2, 3, and 4, respectively. The pump and the probe beams are then recombined with a beam splitter BS, and are focused down onto the front face of a standard laser ruby crystal (diameter = 10 mm and length = 90 mm) by a 300 mm focal length spherical lens L2. The setup is assembled so that the pump and the probe beams are at a small angle, yet are spatially overlapped over the whole length of the sample. The brushless rotating motor (RM) allows us to set the speed of the ruby rotation in a range from 0 to 60 Hz by a digital speed control software and a standard desktop computer. The RM drives the rotation of the ruby by a system of a toothed belt and two gears placed one on the ruby and the other on the motor shaft. The ruby crystal is supported by a high-speed ball bearing system to reduce the friction as it rotates. The pinhole PH3 blocks the transmitted pump beam at the output, and the detector D collects the transmitted probe intensity $I(\Omega)$. The filter F removes any transmitted signal caused by fluorescence in the 600 nm region.

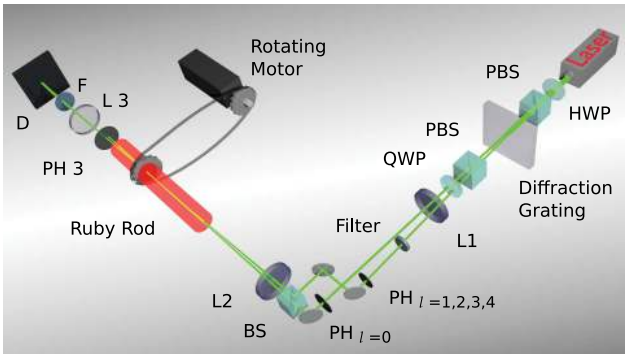

Fig. 1. Schematics of the experimental setup. A CW 532 nm laser beam passes through a diffraction grating to convert the incident plane wave into transmitted helically phased beams of OAM ℓ at the ℓ order diffracted beam. The ℓ state transmitted beam has a diffraction angle of $\Delta\theta = l \cdot \theta$ with $\theta = 1°$. The two beams are focused down onto the ruby front face and axially transmitted. Then the outcoming probe beam is collected by the detector. The rotation of the ruby rod about its axis is controlled by a brushless RM up to ±60 Hz by a digital speed control software.

The experimental results are shown in Fig. 2 where we show the normalized relative transmission T_{norm} (i.e., we subtract the minimum transmitted intensity for varying Ω and then normalize to one) of the probe output intensity for different values of OAM as a function of the rotational speed of the ruby up to ±60 Hz. The rotating ruby medium will rotationally Doppler shift only the probe beam, and the sign of the frequency shift depends on the handedness between the OAM state and the rotation direction; thus, we investigate both sidebands ($\Omega > 0$ and $\Omega < 0$) by changing the direction of rotation. The results show how the mechanical rotation induces a loss that increases with the magnitude of the mechanical rotation. Moreover, the results show that the absorption rate increases for increasing OAM. As also can be seen in Fig. 2, the transmitted intensity T_{norm} has an evident Lorentzian-like dependence (red solid lines) on the rotation speed for all the OAM states, a dependence that we qualitatively justify below.

One may intuit the Lorentzian response of our system using either the coherent population oscillation model of Ref. [17] or the incoherent bleaching model of Ref. [20]. In both cases, the small signal gain seen by a weak detuned probe in the presence of a strong pump of intensity I_1 may be expressed as

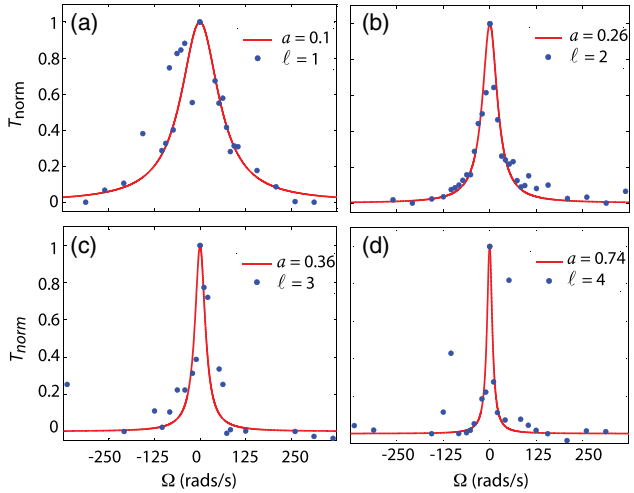

Fig. 2. Normalized relative transmitted intensity T_{norm} of the probe beam as a function of the rotational speed Ω of the ruby for four different OAM states. The blue circles represent the observed transmitted intensity of four different OAM values $\ell = 1$ to 4 (a–d), as indicated in the figures. The solid red line represents the best fits obtained for the Lorentzian phenomenological curve Eq. (5) with the value of the parameter a indicated in each graph.

$$\alpha(\Delta\omega) = \frac{\alpha_0}{1+I_0} - \frac{\alpha_0 I_0}{(T_1\Delta\omega)^2 + (1+I_0)^2}, \quad (3)$$

where $I_0 = I_1/I_{\text{sat}}$ with I_{sat} being the saturation intensity of 1500 kW/cm^2 [25], α_0 being the unsaturated small-signal gain, and T_1 being the ground state recovery time. Applied to the results in Fig. 2 using a Gaussian pump and probe of OAM ℓ, we further set $\Delta\omega = \Omega\ell$. Then, from Eq. (3), we clearly see that, all other factors being equal, the minimum absorption and peak transmission should occur at zero rotation rate, as observed in the experiments. In addition, the second term in Eq. (3) also reveals the Lorentzian dependence on rotation rate that appears in the experiments. However, due to the fact that the beams used in the experiment have transverse intensity profiles, and there is a small angle between the pump and probe beams (meaning that the probe beam is a superposition of OAM states centered on ℓ with respect to the pump beam direction [26]), we cannot appeal directly to Eq. (3) to simulate the data. Rather, motivated by Eq. (3), and noting that the second term is small compared to the first for $I_0 \ll 1$, then the transmitted intensity can be approximated as (neglecting for simplicity in notation the length dependence of $I_0(z)$ as this does not change the form of the final result)

$$I_T = I_0 e^{-\alpha(\Delta\omega)L} \simeq I_0 e^{-\frac{\alpha_0 L}{1+I_0}} + \frac{\alpha_0 L I_0^2}{(T_1\Delta\omega)^2 + (1+I_0)^2}$$

$$\simeq I_0 e^{-\frac{\alpha_0 L}{1+I_0}} + \frac{\alpha_0 L I_0^2}{1+(a\Omega)^2}. \quad (4)$$

In the measurements, we subtract out the unmodulated contribution $I_0 e^{-\frac{\alpha_0 L}{1+I_0}}$ and then normalize, thus obtaining the relative normalized transmission, T_{norm}, discussed above, and that we approximate with a Lorentzian fit:

$$T_{\text{norm}} = \frac{1}{1+(a\Omega)^2}, \quad (5)$$

where $a = \text{const} \times \ell$ depends linearly on the OAM value. This approach is justified by the data as, indeed, this is in good agreement with the phenomenological Lorentzian curve. The parameter a quantifies the decay rate for different OAM states: we obtain $a = 0.1, 0.26, 0.36, 0.74$ s for $\ell = 1, 2, 3, 4$, respectively, demonstrating a differential absorption rate for different OAM probe states induced by the rotation.

Finally, based on Eq. (5), we fit the values of a obtained from the experimental data using a linear function in the form of $a = \text{const} \times \ell$. The observed values and the resulting fit are able to fit the data relatively well, as shown in Fig. 3, with const $= 0.13 \pm 0.017$ s. We also notice an increase in the measurement error for higher ℓ that we ascribe to the fact that the higher OAM modes are characterized by a larger ring diameter, thus overlapping with the outer and noisier regions of the Gaussian pump beam.

In summary, we have provided an example of how the rotational Doppler effect can enter into nonlinear light-matter interactions due to external rotation of the medium. This effect leads to a differential absorption rate for different OAM probe states induced by the mechanical rotation of the medium. Considering that the medium is becoming more opaque with the magnitude of the mechanical rotation, this could be used as a method to control the absorption rate of OAM beams in rotating media by the rotational speed and the OAM states and, for example, providing an alternative route to the remote measurement of a spinning object's rotational rate.

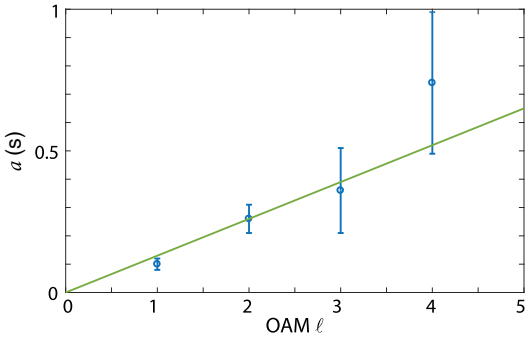

Fig. 3. (Blue circles) observed values of the decay rate parameter a. According to Eq. (5), the decay rate has a linear behavior in the form $a = \text{const} \times \ell$ as a function of the OAM states ℓ (green line). The error bars are indicated with 95% confidence bounds.

Funding. Engineering and Physical Sciences Research Council (EPSRC) (EP/P006078/2).

Acknowledgment. D. F. acknowledges financial support from the EPSRC UK.

REFERENCES

1. B. A. Garetz, J. Opt. Soc. Am. **71**, 609 (1981).
2. M. P. Lavery, S. M. Barnett, F. C. Speirits, and M. J. Padgett, Optica **1**, 1 (2014).
3. S. Barreiro, J. Tabosa, H. Failache, and A. Lezama, Phys. Rev. Lett. **97**, 113601 (2006).
4. J. Courtial, D. Robertson, K. Dholakia, L. Allen, and M. Padgett, Phys. Rev. Lett. **81**, 4828 (1998).
5. M. P. Lavery, F. C. Speirits, S. M. Barnett, and M. J. Padgett, Science **341**, 537 (2013).
6. C. Rosales-Guzmán, N. Hermosa, A. Belmonte, and J. P. Torres, Sci. Rep. **3**, 2815 (2013).
7. L. Allen, M. Babiker, and W. Power, Opt. Commun. **112**, 141 (1994).
8. G. Li, T. Zentgraf, and S. Zhang, Nat. Phys. **12**, 736 (2016).
9. D. Faccio and E. Wright, Phys. Rev. Lett. **118**, 093901 (2017).
10. M. Padgett, G. Whyte, J. Girkin, A. Wright, L. Allen, P. Öhberg, and S. M. Barnett, Opt. Lett. **31**, 2205 (2006).
11. L. Allen and M. Padgett, J. Mod. Opt. **54**, 487 (2007).
12. J. B. Götte, S. M. Barnett, and M. Padgett, Proc. R. Soc. A **463**, 2185 (2007).
13. J. Courtial, K. Dholakia, D. Robertson, L. Allen, and M. Padgett, Phys. Rev. Lett. **80**, 3217 (1998).
14. F. C. Speirits, M. P. Lavery, M. J. Padgett, and S. M. Barnett, Opt. Lett. **39**, 2944 (2014).
15. E. Wisniewski-Barker, G. M. Gibson, S. Franke-Arnold, R. W. Boyd, and M. J. Padgett, Opt. Express **22**, 11690 (2014).
16. E. Wisniewski-Barker, G. Gibson, S. Franke-Arnold, Z. Shi, R. W. Boyd, and M. J. Padgett, New J. Phys. **15**, 083020 (2013).
17. M. S. Bigelow, N. N. Lepeshkin, and R. W. Boyd, Phys. Rev. Lett. **90**, 113903 (2003).
18. R. W. Boyd and D. J. Gauthier, Science **326**, 1074 (2009).
19. M. S. Bigelow, N. N. Lepeshkin, and R. W. Boyd, Science **301**, 200 (2003).
20. B. Macke, I. Razodobreev, and B. Ségard, Phys. Rev. A **95**, 063830 (2017).
21. F. Gires and F. Combaud, J. Phys. **26**, 325 (1965).
22. A. Selden, Br. J. Appl. Phys. **18**, 743 (1967).
23. B. Macke and B. Ségard, Phys. Rev. A **78**, 013817 (2008).
24. R. V. Jones, Proc. R. Soc. A **349**, 423 (1976).
25. P. Liao and D. M. Bloom, Opt. Lett. **3**, 4 (1978).
26. T. Roger, J. J. Heitz, E. M. Wright, and D. Faccio, Sci. Rep. **3**, 3491 (2013).